

Evidence of dual Shapiro steps in a Josephson junctions array

Nicolò Crescini,^{1,*} Samuel Cailleaux,^{1,†} Wiebke Guichard,¹ Cécile Naud,¹ Olivier Buisson,¹ Kater Murch,² and Nicolas Roch^{1,‡}

¹*Univ. Grenoble Alpes, CNRS, Grenoble INP, Institut Néel, 38000 Grenoble, France*

²*Department of Physics, Washington University, St. Louis, Missouri 63130, USA*

(Dated: July 20, 2022)

The modern primary voltage standard is based on the AC Josephson effect and the ensuing Shapiro steps, where a microwave tone applied to a Josephson junction yields a constant voltage $hf/2e$ (h is Planck's constant and e the electron charge) determined by only the microwave frequency f and fundamental constants^{1,2}. Duality arguments for current and voltage³⁻⁹ have long suggested the possibility of dual Shapiro steps—that a Josephson junction device could produce current steps with heights determined only on the applied frequency¹⁰⁻¹³. In this report, we embed an ultrasmall Josephson junction in a high impedance array of larger junctions to reveal dual Shapiro steps⁸. For multiple frequencies, we detect that the AC response of the circuit is synchronised with the microwave tone at frequency f , and the corresponding emergence of flat steps in the DC response with current $2ef$, equal to the tunnelling of a Cooper pair per tone period. This work sheds new light on phase-charge duality, omnipresent in condensed matter physics^{14,15}, and extends it to Josephson circuits. Looking forward, it opens a broad range of possibilities for new experiments in the field of circuit quantum electrodynamics^{16,17} and is an important step towards the long-sought closure of the quantum metrology electrical triangle¹⁸⁻²⁰.

In quantum mechanics, uncertainty relations quantify the incompatibility of quantum operators. For a Josephson junction these operators are the charge Q and the Josephson phase ϕ , which respect $[\phi, Q] = 2ie$, where e is the electron charge²¹. Because of this incompatibility, the suppression of the variance of one of these operators causes the conjugate operator's variance to increase. The balance between phase and charge fluctuations in a junction is determined by the ratio of two energy scales, the Josephson energy $E_J = \hbar I_c/2e$ and the charging energy $E_C = e^2/2C$, where I_c is the critical current of the junction, C is its capacitance and \hbar is the reduced Plank constant²¹. In one limit, $E_J/E_C \gg 1$, the variance of ϕ is small, allowing it to be treated as a classical variable, and the dynamics of the system is described by a tilted washboard potential $U(\phi)$ shown in Fig. 1. By applying a microwave tone, the potential is periodically tilted; one fluxon (Φ_0) is transported across the junction at each period resulting in discrete voltage steps—Shapiro steps—in the IV curve. Au contraire, if $E_J/E_C \lesssim 1$, fluctuations in the phase are enhanced allowing the charge variance to be reduced. In this limit, one expects a microwave drive to produce *dual* Shapiro steps; the cyclical tilting of a potential periodic in charge can meter the transport of Cooper pairs across the junction, resulting in current steps proportional to the applied frequency.

An ultrasmall Josephson junctions (UJJ) has an E_J/E_C ratio smaller than one. The junction Hamiltonian is

$$H = 4E_C (Q/2e)^2 - E_J \cos(\phi), \quad (1)$$

which, using Bloch's theorem²², can be recast to

$$H = \sum_s U^{(s)}(q), \quad (2)$$

where we have introduced the quasicharge q and the Bloch bands $U^{(s)}(q)$ ¹⁰. When this junction is embedded in an environment of impedance R , thermal and quantum fluctuations can further increase the charge variance. Here, charge fluctuations are bounded by the energy-time uncertainty relation $\Delta E \Delta \tau > \hbar$, where the charging time of the junction capacitance is $\Delta \tau = RC$. Hence, large impedance is necessary to reduce the charge fluctuations, in particular to have $\Delta E < E_C$ requires, $R > h/4e^2 \simeq 6.45 \text{ k}\Omega$, the quantum of resistance. Additionally, to suppress thermal fluctuations one has to cool the environment to ultracryogenic temperatures $T < E_C/k_B$. Under these conditions the charge is localised and thus can be treated as a classical variable. Q is well approximated by q as its dynamics is restricted to the first Bloch band ($s = 0$), thereby realising the periodic potential $U(Q) \simeq U^{(0)}(q) = \cos(\pi Q/e)$ —dual to $U(\phi)$ —shown in Fig. 1. The periodic potential corresponds to a nonlinear capacitance—dual to the nonlinear inductance typically associated with a Josephson junction. Table I summarises the dual transformations in Josephson circuits. Along these lines, the amplitude of the first Bloch band is

Dual transformations

$E_J/E_C \gg 1$	$E_J/E_C \leq 1$
Classical (localised) ϕ	Classical (localised) q
Tilted washboard $U(\phi)$	First Bloch band $U(Q)$
Nonlinear inductance	Nonlinear capacitance
Critical current I_c	Critical voltage V_c
AC Josephson effect	Bloch oscillations
Fluxons transport	Cooper pairs transport
Shapiro steps	Dual Shapiro steps

TABLE I. Summary of dual transformations in a Josephson circuit.

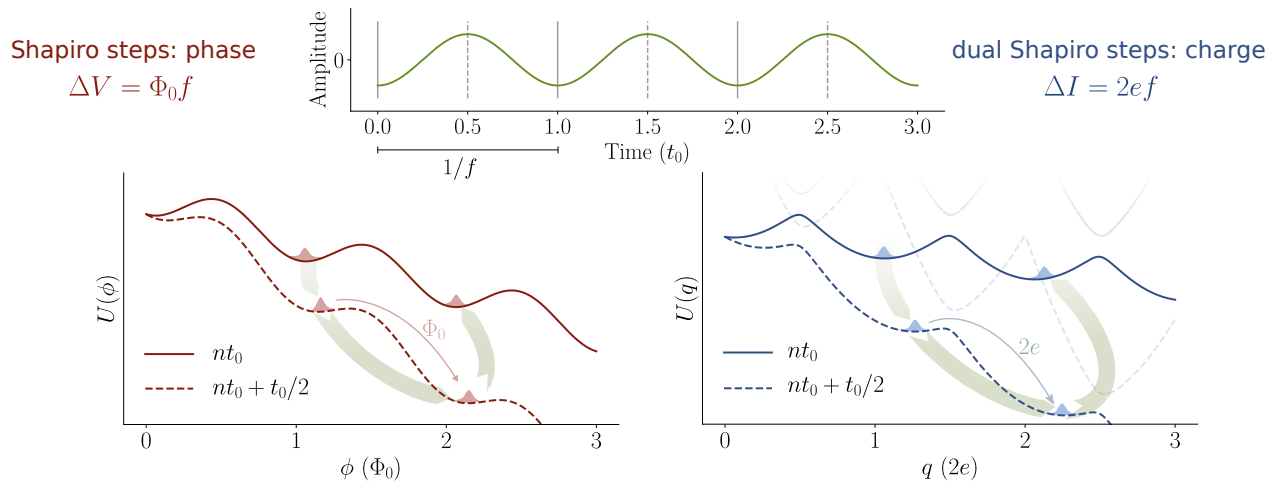


FIG. 1. The Shapiro steps and their dual. Usual Shapiro steps are realised by periodically tilting the washboard potential of a Josephson junction with $E_J \gg E_C$. Since the phase is a well defined variable, the driving of the potential yields steps of constant voltage $\Phi_0 f$ ($\Phi_0 = h/2e$ is the flux quantum) that are precisely determined by the metered transport of fluxons. In contrast, the dual phenomenon (right side) uses the lowest Bloch band of a junction with $E_J \leq E_C$ (higher bands in the picture are shown only for an illustrative purpose). With charge as the well defined variable, current steps of value $2ef$ determined by the cyclic transport of Cooper pairs appear: the dual Shapiro steps.

related to the critical voltage $V_c = \pi E_Q/e$, the minimum voltage required for a flow of DC current across the junction. V_c is dual to the critical current, the current below which no voltage is generated⁶. Upon the application of a DC current, the system exhibits Bloch oscillations^{10,23}, i.e. voltage oscillations arising in the presence of a constant force, a phenomenon dual to the AC Josephson effect. If these oscillations are synchronised with an external tone, they yield dual Shapiro steps^{8,10,24}.

Prior work has demonstrated some of the essential components for the exploration of Josephson circuits' duality. A charge periodic potential has been obtained in UJJs^{23,25–27} or nanowires^{28–31}. Large impedance environments have been realised by using resistors²³, suspended³² or low dielectric constant³³ substrates, high kinetic inductance materials^{28,31,34,35}, or metamaterials^{16,17,36–38}. Despite this progress a clear demonstration of dual Shapiro steps is still missing. In this work, we harness techniques from circuit QED³⁹ to study the interplay of microwave drive and DC bias of an UJJ embedded in a superconducting high-impedance environment. Utilising low noise microwave spectroscopy, we observe the onset of a microwave mode synchronised with an external tone. In turn, we observe current plateaux proportional to the frequency of the microwaves. These two experimental observations are consistent with synchronised Bloch oscillations and dual Shapiro steps.

Fig. 2 shows the device used in this work, which we refer to as a Bloch array, and consists in a superconducting quantum interference device (SQUID) formed by

two ultrasmall junctions surrounded by two linear JJs superinductances which provide the high impedance environment. The array consists of Al/AlO_x/Al junctions in stripline geometry on a fused silica wafer, which reduces the capacitance to ground⁴⁰. The SQUID is formed by junctions of area $0.2 \times 0.2 \mu\text{m}^2$ ($E_J/E_C \simeq 0.4$) each, and the superinductance comprises an array of $N_a/2 = 1750$ junctions with an area of $1 \mu\text{m}^2$ ($E_J/E_C \simeq 250$)⁴¹. From these parameters we estimate a first Bloch band width of $E_Q/h = 2.5$ GHz and a minimum gap of 7.9 GHz between the first and the second Bloch band. Each superinductance's characteristic impedance and inductance are $Z = 8.0 \text{ k}\Omega$ and $L/2 = 3.3 \mu\text{H}$, respectively. A scanning electron microscope (SEM) image is shown in Fig. 2b. Further details are given in the Methods section. The Bloch array is studied with an experimental setup allowing for simultaneous DC and RF measurements, as is shown in Fig. 2c. Measurements are performed at the base temperature of a dilution refrigerator with $T \simeq 23$ mK.

We first examine the DC and RF response of the Bloch array separately. The IV curve is obtained by biasing the device with the voltage V_0 and reading out the corresponding current I_0 . Here we consider $|V_0| \leq 10$ mV while the whole IV curve is described in the Methods section. As is shown in the plot, the current-voltage characteristics exhibits several current peaks^{42,43} evenly spaced by 2Δ , the superconducting gap of aluminium. These peaks can be understood as follows. When a voltage is applied to the Bloch array one of the junctions (J_1) is biased to the sub-gap state, behaving as a large series

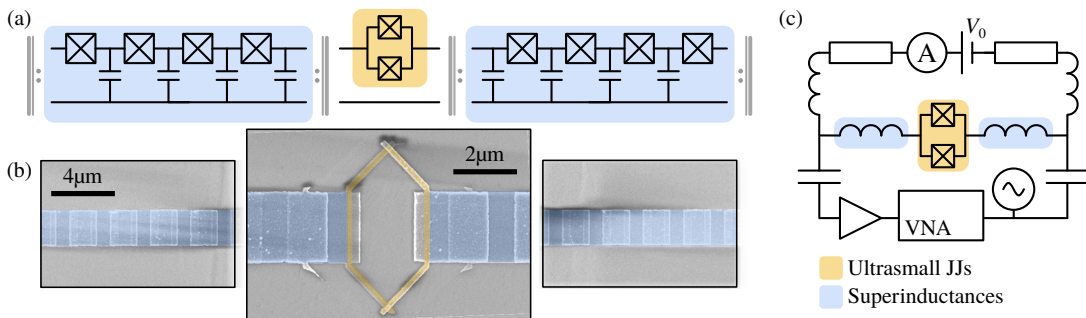


FIG. 2. Overview of device and measurement setup, where the UJJ is shown in orange and the JJ array in blue. (a) Circuit schematic of the Bloch array. (b) SEM image of the UJJ and of the beginning of JJ arrays nominally identical to the one under test. (c) Simplified schematic of the measurement setup including the device, bias tees, damping resistors, DC and RF electronics, and a vector-network analyser (VNA).

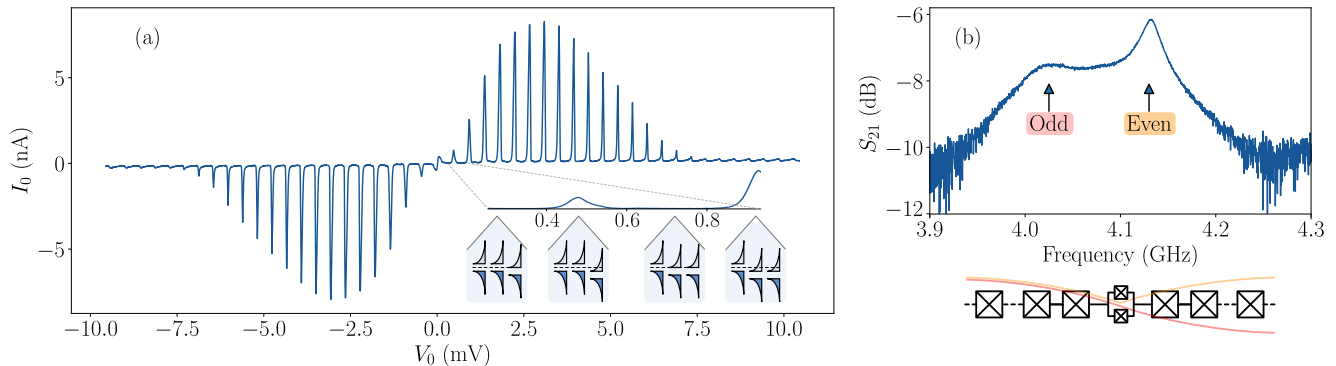


FIG. 3. DC and RF characterisation of the Bloch array. Plot (a) is the low voltage IV curve, which is detailed in the text. The inset schematically shows the switching mechanism of the junctions in the array with a band model, where the dashed line is a guide to the eye. The microwave transmission of the Bloch array's fourth mode doublet is displayed in (b), where the voltage profile of odd and even modes is shown below.

resistance, and the flow of current is suppressed. Consequently, V_0 drops on J_1 until it reaches the gap. When $V_0 = 2\Delta$, J_1 turns normal conducting, and I_0 sharply increases until a second junction J_2 is biased into the sub-gap state, introducing again a large series resistance and suppressing the current. To turn both the junctions resistive the voltage needs to be 4Δ , and the process repeats. A schematic of this mechanism is reported in the inset of Fig. 3a. This successive switching resets the voltage drop across the junctions every 2Δ . In this way the same physics, and in particular the low voltage physics, repeats at voltages modulo 2Δ as one more junction switches to the normal state per step. RCSJ simulations of a voltage biased JJ array, reported in the Methods, are in agreement with our observations.

The microwave transmission of a Bloch array exhibits mode doublets, one with odd and one with even symmetry³⁸, as is shown in Fig. 3b. The odd mode is coupled to the UJJ at the centre of the array, while the even one is not, as is comprehensively discussed by Leger et al.³⁸. The frequency of the odd mode is lower than the even mode, which is consistent with the presence of

a capacitive element between the left and right superinductances. This agrees with duality considerations, according to which the UJJ should behave as a nonlinear capacitance. Leveraging the DC and microwave capabilities of our setup, we investigate the effect of an applied voltage on the modes of the Bloch array. By measuring the S_{21} as a function of V_0 , we observe that between two current peaks the doublet is visible yet starts to degrade when current flows through the array. The mode doublet is replicated after every 2Δ -switch, compatible with the mechanism depicted by the IV curve. The full measurement is detailed in the Methods and in Fig 10.

We now study the behaviour of the Bloch array in the presence of an additional applied microwave tone. In Fig. 4a we display the microwave transmission of the Bloch array near the mode doublet at 4.1 GHz for different frequencies, f , of the microwave tone with power $p = -5.0$ dBm. We observe that the array odd mode is influenced by the microwave tone, and drifts away from f , in a mode repulsion fashion. A mode synchronous with the pump appears when the frequency exceeds $\simeq 4.02$ GHz, and fades around $f \simeq 4.11$ GHz. This behaviour is fur-

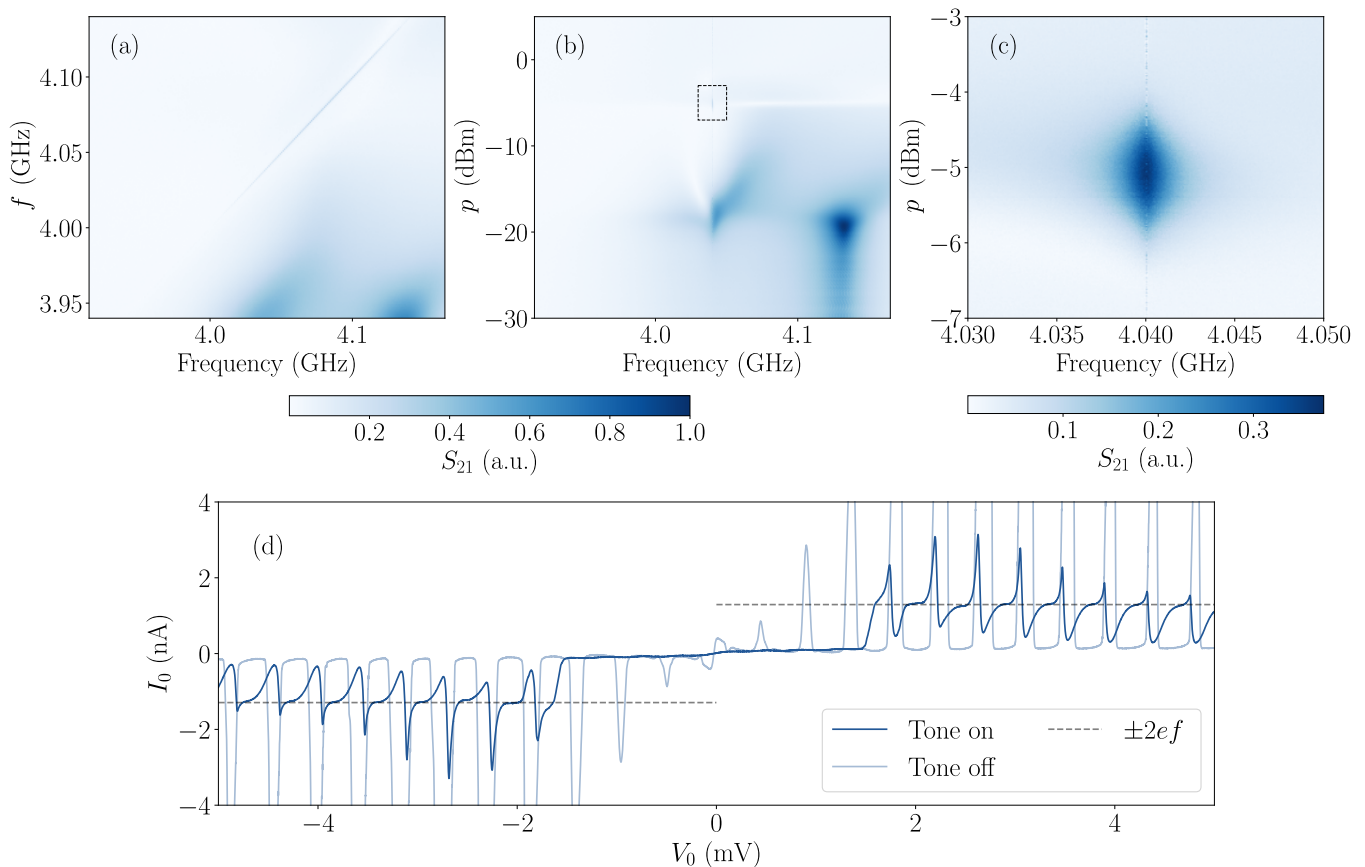


FIG. 4. Emergence of Bloch oscillations and dual Shapiro steps. In (a) the frequency of the external tone f is changed to observe the effect it has on the transmission spectrum of the Bloch array. A similar measurement is reported in (b) where we vary the power p of the tone at fixed frequency $f = 4.04$ GHz. The dashed rectangle evidences the plot region reported in (c), where the transition between tone interference and microwave mode is clearly visible. Plot (d) shows the IV characteristics measured for $f = 4.04$ GHz and $p = -5.0$ dBm. Between two current peaks the plateaux current is $\pm 2ef$, as is evidenced by the grey dashed lines.

ther studied by varying p at $f = 4.04$ GHz, as reported in Fig. 4b. At low power the array is essentially unaltered by the tone, until p reaches -20 dBm and the spectrum shows a profile corresponding to a Fano resonance, whose maximum-to-minimum separation increases with p . The most noteworthy feature is at $p \simeq -5$ dBm, which is presented in Fig. 4c. We clearly observe a microwave mode with a Lorentzian shape and linewidth of about 1 MHz, centered at f , which disappears at higher p . We refer to this feature as a Bloch mode, as it is consistent with Bloch oscillations synchronised with the external tone⁴⁴.

Focusing on this microwave synchronised Bloch mode ($f = 4.04$ GHz, $p = -5.0$ dBm), we now examine the IV characteristic of the Bloch array under microwave irradiation as displayed in Fig. 4d. The IV presents a wide central region with no current or supercurrent peaks. Outside this central part, we observe that for both positive and negative voltage, current plateaux form before the 2Δ current peaks. The current corresponding to their flat part is $2ef$ within a 0.1% accuracy. These observa-

tions are supported by simulations (see Methods) showing that the steps should emerge as a flat current region right before the upward slope of the 2Δ peaks.

Figure 5 displays a more detailed investigation of these current steps. In Fig. 5a we display the heights of three different current plateaux versus p , which have a saturation point at $p = -5$ dBm, and $I_0 = 2ef$. The tone power p influences the height of the step and quantized flat steps are obtained only for a given power range, in a fashion very similar to what is observed for standard Shapiro steps⁴⁵. To further assess the stability of the step, we modulate the microwave power p and measure the corresponding I_0 variation with a lock-in amplifier. The result is displayed in Fig. 5b and shows that dI_0/dp falls to the noise floor at $p \simeq -5$ dBm, suggesting a current that is independent of the microwave power.

Microwave power is delivered to the UJJ when the tone is on resonance with the odd microwave mode of the array. Utilising microwave spectroscopy, we identify other suitable working points (see Methods), correspond-

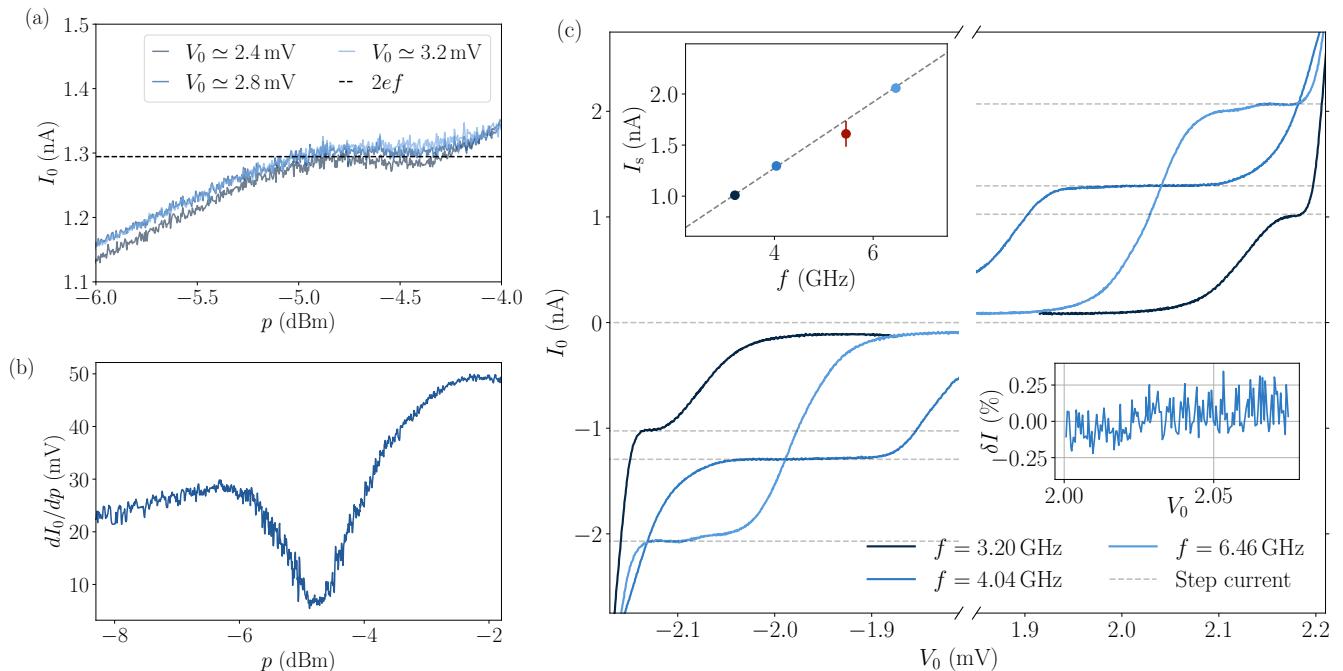


FIG. 5. Current plateaux at different microwave tone frequency and power. (a) Average plateaux current at different microwave powers p for three separate voltages. (b) Lock-in measurement collected by modulating the microwave power p and detecting the corresponding current variation at $V_0 = 2.4$ mV. (c) For three different values of f we follow the procedure described in the text to observe current plateaux whose amplitude correspond to the one of the first dual Shapiro step, which is shown as a grey dashed line. The inset shows the relation between the step current I_s and tone frequency, and the fitted slope is consisted with $2e$. The red point's IV curve was omitted for clarity (see the main text and the Methods for further details).

ing to different mode doublets of the Bloch array. In Fig. 5c, we display the lowest bias voltage current step common to three additional frequencies. The parameters and additional measurements used to obtain these curves are detailed in the Methods section. For a total of four mode frequencies, we observe that I_0 flattens at the corresponding $2ef$ for $f = 3.20$ GHz, 4.04 GHz, 5.45 GHz and 6.46 GHz. Finally, the inset of Fig. 5c shows the frequency dependence of I_s , the average current on the flat part of each step. Through the slope of the fitting line we can estimate a Cooper pair's charge of $(3.23 \pm 0.07) \times 10^{-19}$ C. Even though the measurement was not optimised, the average deviation from the expected current $\delta I = I_0/2ef - 1$ on the 4 GHz step is $\langle \delta I^2 \rangle^{1/2} \leq 0.001$, limited by the setup noise in an averaging time of one minute (see inset of Fig. 5c).

The environment of the UJJ, formed by the Josephson junction arrays, does more than provide the required high impedance for charge localisation. As we have discussed, the switching of the junctions in the array absorbs the majority of the applied voltage, allowing the UJJ to remain in the superconducting state even at high V_0 . Furthermore, the microwave response of the device allows us to selectively apply a microwave drive to the UJJ, causing the formation of the Bloch mode and the corresponding onset of current steps. In contrast, no ef-

fect is observed when driving the even mode which does not couple to the UJJ.

Our work highlights how the Bloch array can be harnessed to engineer dissipation, thereby resolving charge at the expense of phase fluctuations, a regime dual of what is commonly achieved in Josephson circuits (localised phase and large charge fluctuations). We take advantage of this new configuration and observe quantised current steps: dual Shapiro steps. The quantum metrology electrical triangle links current, voltage, and frequency via three quantum effects. Voltage and frequency can be related via the AC Josephson effect, while current and voltage via the quantum Hall effect. Here we study the third edge of the triangle by relating current and frequency via the charge $2e$ of a Cooper pair. This first step in this direction indicates the rich physics of the Bloch array will have to be fully mastered in the process of developing the dual Josephson effect into a metrological definition of the Ampère^{19,46}. This also opens exciting opportunities from the perspective of fundamental physics via tests of quantum electrodynamics through the closure of the triangle⁴⁷ or further exploration of phase charge duality in Josephson devices.

Acknowledgements – The help of Denis Basko is deeply acknowledged and appreciated. The support of the superconducting circuits team of Institut Néel is warmly

acknowledged. The authors are also grateful to Joe Aumentado, Michel Devoret, Tim Duty, Serge Florens, David Haviland, Julien Renard, Benjamin Sacepe and Izak Snyman for the fruitful discussion and comments on our work. Furthermore, our gratitude goes to the members of the Triangle consortium, namely Philippe Joyez, Çağlar Girit, Cristiano Ciuti, Helene Le Sueur and Alexander Wagner, for the valuable discussion and insights. The samples were fabricated in the clean room facility of Institute Néel, Grenoble; we would like to thank all the staff for help with the devices fabrication. We would like to acknowledge Eric Eyraud for his help in the installation of the experimental setup. This work was supported by the French National Research Agency (ANR) in the framework of the TRIANGLE project (ANR-20-CE47-0011). N.C. is supported by the European Union's Horizon 2020 research and innovation program under the Marie Skłodowska-Curie grant agreement QMET No. 101029189. K.W.M acknowledges support from NSF Grant No. PHY-1752844 (CAREER), AFOSR MURI Grant No. FA9550-21-1-0202, and ONR Grant No. N00014-21-1-2630.

During the writing of this work, we became aware that the group of Evgeni Il'ichev and Oleg Astafiev observed quantised current steps in a superconducting nanowires system. We would like to thank them for the discussion and their comments.

* nicolo.crescini@neel.cnrs.fr; the authors contributed equally to this work.

† samuel.cailleaux@neel.cnrs.fr; the authors contributed equally to this work.

‡ nicolas.roch@neel.cnrs.fr

- [1] B. D. Josephson. Possible new effects in superconductive tunnelling. *Physics Letters*, 1(7):251–253, July 1962.
- [2] Sidney Shapiro. Josephson Currents in Superconducting Tunneling: The Effect of Microwaves and Other Observations. *Physical Review Letters*, 11(2):80–82, July 1963.
- [3] Gerd Schön and A.D. Zaikin. Quantum coherent effects, phase transitions, and the dissipative dynamics of ultra small tunnel junctions. *Physics Reports*, 198(5-6):237–412, December 1990.
- [4] T. P. Spiller, T. D. Clark, R. J. Prance, H. Prance, and D. A. Poulton. Electromagnetic duality in quantum circuits. *Il Nuovo Cimento B Series 11*, 105(1):43–52, January 1990.
- [5] Gert-Ludwig Ingold and Yu. V. Nazarov. Charge Tunneling Rates in Ultrasmall Junctions. In Hermann Grabert and Michel H. Devoret, editors, *Single Charge Tunneling: Coulomb Blockade Phenomena In Nanostructures*, pages 21–107. Springer US, Boston, MA, 1992.
- [6] S. Corlevi, W. Guichard, F. W. J. Hekking, and D. B. Haviland. Phase-Charge Duality of a Josephson Junction in a Fluctuating Electromagnetic Environment. *Physical Review Letters*, 97(9):096802, August 2006.
- [7] K.Yu. Arutyunov, D.S. Golubev, and A.D. Zaikin. Superconductivity in one dimension. *Physics Reports*, 464(1-2):1–70, July 2008.
- [8] W. Guichard and F. W. J. Hekking. Phase-charge duality in Josephson junction circuits: Role of inertia and effect of microwave irradiation. *Physical Review B*, 81(6):064508, February 2010.
- [9] Andrew J Kerman. Flux–charge duality and topological quantum phase fluctuations in quasi-one-dimensional superconductors. *New Journal of Physics*, 15(10):105017, October 2013.
- [10] K. K. Likharev and A. B. Zorin. Theory of the Bloch-wave oscillations in small Josephson junctions. *Journal of Low Temperature Physics*, 59(3-4):347–382, May 1985.
- [11] D V Averin, A B Zorin, and K K Likharev. Bloch oscillations in small Josephson junctions. *Sov. Phys. JETP*, 61(2):7, February 1985.
- [12] D.V. Averin and A.A. Odintsov. Phase locking of the Bloch oscillations in ultrasmall Josephson junctions. *Physica B: Condensed Matter*, 165-166:935–936, 1990. LT-19.
- [13] G. Y. Hu and R. F. O’Connell. Bloch oscillations in small-capacitance Josephson junctions. *Physical Review B*, 47(14):8823–8830, April 1993.
- [14] D. Shahar, D. C. Tsui, M. Shayegan, E. Shimshoni, and S. L. Sondhi. Evidence for Charge-Flux Duality near the Quantum Hall Liquid-to-Insulator Transition. *Science*, 274(5287):589–592, 1996.
- [15] Maoz Ovadia, David Kalok, Benjamin Sacépé, and Dan Shahar. Duality symmetry and its breakdown in the vicinity of the superconductor–insulator transition. *Nature Physics*, 9(7):415–418, 2013.
- [16] Javier Puertas Martínez, Sébastien Léger, Nicolas Gheeraert, Rémy Dassonneville, Luca Planat, Farshad Foroughi, Yuriy Krupko, Olivier Buisson, Cécile Naud, Wiebke Hasch-Guichard, Serge Florens, Izak Snyman, and Nicolas Roch. A tunable Josephson platform to explore many-body quantum optics in circuit-QED. *npj Quantum Information*, 5(1):19, December 2019.
- [17] Ivan V. Pechenezhskiy, Raymond A. Mencia, Long B. Nguyen, Yen-Hsiang Lin, and Vladimir E. Manucharyan. The superconducting quasicharge qubit. *Nature*, 585(7825):368–371, September 2020.
- [18] K. Likharev and A. Zorin. Bloch oscillations in small Josephson junctions: Possible fundamental standard of dc current and other applications. *IEEE Transactions on Magnetics*, 21(2):943–946, March 1985. Conference Name: IEEE Transactions on Magnetics.
- [19] Jukka P. Pekola, Olli-Pentti Saira, Ville F. Maisi, Antti Kemppinen, Mikko Möttönen, Yuri A. Pashkin, and Dmitri V. Averin. Single-electron current sources: Toward a refined definition of the ampere. *Reviews of Modern Physics*, 85(4):1421–1472, October 2013.
- [20] Jonas Bylander, Tim Duty, and Per Delsing. Current measurement by real-time counting of single electrons. *Nature*, 434(7031):361–364, March 2005.
- [21] Michael Tinkham. *Introduction to Superconductivity*. Dover Publications, 2 edition, June 2004.
- [22] Neil W Ashcroft and N David Mermin. *Solid state physics*. Holt, Rinehart and Winston, New York, NY, 1976.
- [23] L. Kuzmin and D. Haviland. Observation of the Bloch oscillations in an ultrasmall Josephson junction. *Physical Review Letters*, 67(20):2890–2893, November 1991.
- [24] A. Di Marco, F. W. J. Hekking, and G. Rastelli. Quantum phase-slip junction under microwave irradiation.

- Physical Review B*, 91(18):184512, May 2015.
- [25] Karin Andersson, Per Delsing, and David Haviland. Synchronous Cooper pair tunneling in a 1D-array of Josephson junctions. *Physica B: Condensed Matter*, 284-288:1816–1817, July 2000.
- [26] T. Weißl, G. Rastelli, I. Matei, I. M. Pop, O. Buisson, F. W. J. Hekking, and W. Guichard. Bloch band dynamics of a Josephson junction in an inductive environment. *Physical Review B*, 91(1):014507, January 2015.
- [27] Karin Cedergren, Roger Ackroyd, Sergey Kafanov, Nicolas Vogt, Alexander Shnirman, and Timothy Duty. Insulating Josephson Junction Chains as Pinned Luttinger Liquids. *Physical Review Letters*, 119(16):167701, October 2017.
- [28] C. N. Lau, N. Markovic, M. Bockrath, A. Bezryadin, and M. Tinkham. Quantum Phase Slips in Superconducting Nanowires. *Physical Review Letters*, 87(21):217003, November 2001.
- [29] J. S. Lehtinen, K. Zakharov, and K. Yu. Arutyunov. Coulomb Blockade and Bloch Oscillations in Superconducting Ti Nanowires. *Physical Review Letters*, 109(18):187001, October 2012.
- [30] Zhiming M. Wang, J. S. Lehtinen, and K. Yu. Arutyunov. Towards quantum phase slip based standard of electric current. *Applied Physics Letters*, 114(24):242601, 2019.
- [31] C. H. Webster, J. C. Fenton, T. T. Hongisto, S. P. Giblin, A. B. Zorin, and P. A. Warburton. Nbsi nanowire quantum phase-slip circuits: dc supercurrent blockade, microwave measurements, and thermal analysis. *Phys. Rev. B*, 87:144510, Apr 2013.
- [32] Matilda Peruzzo, Farid Hassani, Gregory Szep, Andrea Trioni, Elena Redchenko, Martin Žemlička, and Johannes M. Fink. Geometric Superinductance Qubits: Controlling Phase Delocalization across a Single Josephson Junction. *PRX Quantum*, 2(4):040341, November 2021.
- [33] C Rolland, A Peugeot, S Dambach, M Westig, B Kubala, Y Mukharsky, C Altimiras, H le Sueur, P Joyez, D Vion, P Roche, D Esteve, J Ankerhold, and F Portier. Antibunched Photons Emitted by a dc-Biased Josephson Junction. *Physical Review Letters*, 122(18):186804, 05 2019.
- [34] Kazuo Yoshihiro. Observation of “Bloch oscillations” in granular tin films. *Physica B: Condensed Matter*, 152(1-2):207–211, August 1988.
- [35] Lukas Grünhaupt, Martin Spiecker, Daria Gusenkova, Nataliya Maleeva, Sebastian T. Skacel, Ivan Takmakov, Francesco Valenti, Patrick Winkel, Hannes Rotzinger, Wolfgang Wernsdorfer, Alexey V. Ustinov, and Ioan M. Pop. Granular aluminium as a superconducting material for high-impedance quantum circuits. *Nature Materials*, 18(8):816–819, August 2019. Number: 8 Publisher: Nature Publishing Group.
- [36] M. Bell, I. Sadovskyy, L. Ioffe, A. Kitaev, and M. Gershenson. Quantum Superinductor with Tunable Nonlinearity. *Physical Review Letters*, 109:137003, 09 2012.
- [37] Nicholas Masluk, Ioan Pop, Archana Kamal, Zlatko Minev, and Michel Devoret. Microwave Characterization of Josephson Junction Arrays: Implementing a Low Loss Superinductance. *Physical Review Letters*, 109:137002, 09 2012.
- [38] Sébastien Léger, Javier Puertas-Martínez, Karthik Bharadwaj, Rémy Dassonneville, Jovian Delaforce, Farshad Foroughi, Vladimir Milchakov, Luca Planat, Olivier Buisson, Cécile Naud, Wiebke Hasch-Guichard, Serge Florens, Izak Snyman, and Nicolas Roch. Observation of quantum many-body effects due to zero point fluctuations in superconducting circuits. *Nature Communications*, 10(1):5259, December 2019.
- [39] Alexandre Blais, Arne L. Grimsmo, S. M. Girvin, and Andreas Wallraff. Circuit quantum electrodynamics. *Rev. Mod. Phys.*, 93:025005, May 2021.
- [40] Lisa Arndt, Ananda Roy, and Fabian Hassler. Dual Shapiro steps of a phase-slip junction in the presence of a parasitic capacitance. *Physical Review B*, 98(1):014525, July 2018.
- [41] The array’s first junctions reported in the figure are slightly larger than the ones in the rest of the device (not shown). This is not expected to result in any difference.
- [42] David B. Haviland, Karin Andersson, and Peter Ågren. Superconducting and Insulating Behavior in One-Dimensional Josephson Junction Arrays. *Journal of Low Temperature Physics*, 118(5):733–749, March 2000.
- [43] R. Dolata, H. Scherer, A. B. Zorin, and J. Niemeyer. Single-charge devices with ultrasmall Nb/AlO_x/Nb trilayer Josephson junctions. *Journal of Applied Physics*, 97(5):054501, March 2005.
- [44] G. Lenz, I. Talanina, and C. Martijn de Sterke. Bloch Oscillations in an Array of Curved Optical Waveguides. *Physical Review Letters*, 83(5):963–966, August 1999.
- [45] Kévin Le Calvez, Louis Veyrat, Frédéric Gay, Philippe Plaindoux, Clemens B. Winkelmann, Hervé Courtois, and Benjamin Sacépé. Joule overheating poisons the fractional ac Josephson effect in topological Josephson junctions. *Communications Physics*, 2(1):4, 2019.
- [46] E. O. Göbel and U Siegner. *The New International System of Units (SI) – Quantum Metrology and Quantum Standards*. John Wiley & Sons, Ltd, 2019.
- [47] Tim Sailer, Vincent Debierre, Zoltán Harman, Fabian Heiße, Charlotte König, Jonathan Morgner, Bingsheng Tu, Andrey V. Volotka, Christoph H. Keitel, Klaus Blaum, and Sven Sturm. Measurement of the bound-electron g-factor difference in coupled ions. *Nature*, 606(7914):479–483, June 2022.
- [48] Clark A. Hamilton. Josephson voltage standards. *Review of Scientific Instruments*, 71(10):3611–3623, 2000.
- [49] Jens Koch, Terri M. Yu, Jay Gambetta, A. A. Houck, D. I. Schuster, J. Majer, Alexandre Blais, M. H. Devoret, S. M. Girvin, and R. J. Schoelkopf. Charge-insensitive qubit design derived from the cooper pair box. *Phys. Rev. A*, 76:042319, Oct 2007.
- [50] J. A. Schreier, A. A. Houck, Jens Koch, D. I. Schuster, B. R. Johnson, J. M. Chow, J. M. Gambetta, J. Majer, L. Frunzio, M. H. Devoret, S. M. Girvin, and R. J. Schoelkopf. Suppressing charge noise decoherence in superconducting charge qubits. *Phys. Rev. B*, 77:180502, May 2008.
- [51] The DOI for a data repository will be inserted upon the acceptance of the manuscript.
- [52] N A Court, A J Ferguson, and R G Clark. Energy gap measurement of nanostructured aluminium thin films for single cooper-pair devices. *Superconductor Science and Technology*, 21(1):015013, nov 2007.
- [53] Adem Ergül, David Schaeffer, Magnus Lindblom, David B. Haviland, Jack Lidmar, and Jan Johansson. Phase sticking in one-dimensional Josephson junction chains. *Physical Review B*, 88(10):104501, September 2013.

- [54] Juha Leppäkangas, Mikael Fogelström, Alexander Grimm, Max Hofheinz, Michael Marthaler, and Göran Johansson. Antibunched photons from inelastic cooper-pair tunneling. *Phys. Rev. Lett.*, 115:027004, Jul 2015.
- [55] M. Hofheinz, F. Portier, Q. Baudouin, P. Joyez, D. Vion, P. Bertet, P. Roche, and D. Esteve. Bright side of the coulomb blockade. *Phys. Rev. Lett.*, 106:217005, May 2011.
- [56] Yu Krupko, V D Nguyen, T Weissl, E Dumur, J Puertas, R Dassonneville, C Naud, F W J Hekking, D M Basko, O Buisson, N Roch, and W Hasch-Guichard. Kerr non-linearity in a superconducting Josephson metamaterial. *Phys Rev B*, 98(9):094516, 09 2018.

METHODS

The Methods sections are organised as follows. In the first two sections we describe the phase charge duality and a semiclassical model that can give intuition into the observations, and simulation results from a minimal a RCSJ model. In the third section we detail the device fabrication, parameters and experimental measurement setup. The fourth section presents the full IV curve of the device as well as its flux dependence, while the fifth one describes the microwave properties of the device. The last two sections display the characterisation of the microwave modes used for the observation of the current steps and their power and flux dependence.

Semiclassical model and exact duality

The two energy scales in a Josephson junction are the Josephson energy E_J and the charging energy E_C . A large E_J/E_C ratio is used, for example for the Josephson voltage standard⁴⁸ or in transmon qubits^{49,50}, where an almost classical behaviour of the superconducting phase is favourable. When $E_J \lesssim E_C$, the charge of a single electron is relevant, and quantum phase fluctuations are not negligible. In this regime, charge dynamics can be dual to the Josephson phase dynamics, provided that the environmental impedance and inductance L are large^{8,24,40}. Eq. (1) describes a particle in a one-dimensional lattice, whose spectrum consists of Bloch bands²², as shown in Fig. 1. If the dynamics is restricted to the first Bloch band, and the bath response is ohmic with resistance

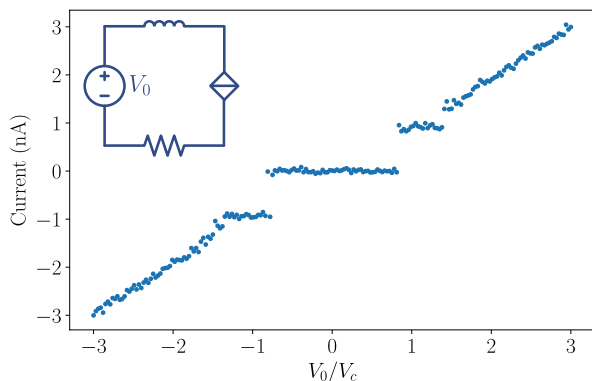


FIG. 6. Simulation of the CJLR circuit under microwave irradiation with experimental noise. This IV curves are used to determine how clear are the steps for different parameters combinations and do not resemble the actual steps observed in our device. The inset is the simulated circuit, where the diamond is the non-linear capacitor ($\cos(\frac{\pi}{e}Q)$ element).

R^8 , the equation of motion for the charge is given by

$$L\ddot{Q} + R\dot{Q} + V_c \sin\left(\frac{\pi}{e}Q\right) = V_0 + V_1, \quad (3)$$

where V_c is the critical voltage of the junction, $V_0 + V_1$ are the DC and AC applied voltages, respectively, and the shape of the first Bloch band is approximated as $\cos(\pi Q/e)$. Eq. 3 is the exact dual to the equation of motion of a large E_J/E_C ratio JJ. While Eq. 3 does not accurately model the complex physics of the Bloch array, it does provide useful intuition and serves as a guide for choosing the system parameters.

Following the work of Guichard and Hekking⁸, we calculate the time evolution of the system for a fixed voltage, allowing us to produce the IV characteristic of the circuit as reported in Fig. 6. The CJRL system under consideration is reported in the lumped element schematic in the inset of Fig. 6. The usual phase dynamics associated with the Josephson tunneling is replaced by its dual counterpart: the quasicharge dynamics. In this way, instead of the voltage Shapiro steps, one can expect quantised current steps. As with prior work⁸, here the signal is perturbed with the voltage noise of the resistor and of the readout amplifier. The circuit parameters are the same as the ones in the main text.

RCSJ toy model

The IV curve of the array is simulated by numerically solving the equations of motion of a chain of N junctions in series with a non-linear capacitor, an inductance and a damping resistor under a voltage drive. Each junction is modeled using the resistively and capacitively shunted junction model (RCSJ). The total current I_{tot} through a junction is thus the sum of a capacitive current I_C , a resistive current I_R and a Josephson current I_J :

$$\begin{aligned} I_{\text{tot}} &= I_C + I_R + I_J, \\ I_C &= C\ddot{\phi}_i, \\ I_R &= s(\dot{\phi}_i) \frac{1}{R_N} \dot{\phi}_i, \\ I_J &= \left(1 - s(\dot{\phi}_i)\right) I_c \sin\left(\frac{\phi_i}{\phi_0}\right). \end{aligned} \quad (4)$$

In Eqs. (4), ϕ_i is the superconducting flux drop across the i^{th} junction, R_N is its normal state resistance, C is its capacitance and I_c its critical current. We model the gap transition of the junction through the factor $s(\dot{\phi}_i)$ which goes smoothly from 0 when $|\dot{\phi}_i| < 2\Delta$ to 1 when $|\dot{\phi}_i| > 2\Delta$. We found that the exact shape of the function s does not impact the resulting IV characteristics as long as the transition is sharp. All the results presented used a scaled sigmoid for the transition function. The charge and its associated current $I_{\text{tot}} = \dot{Q}$ are related to the bias

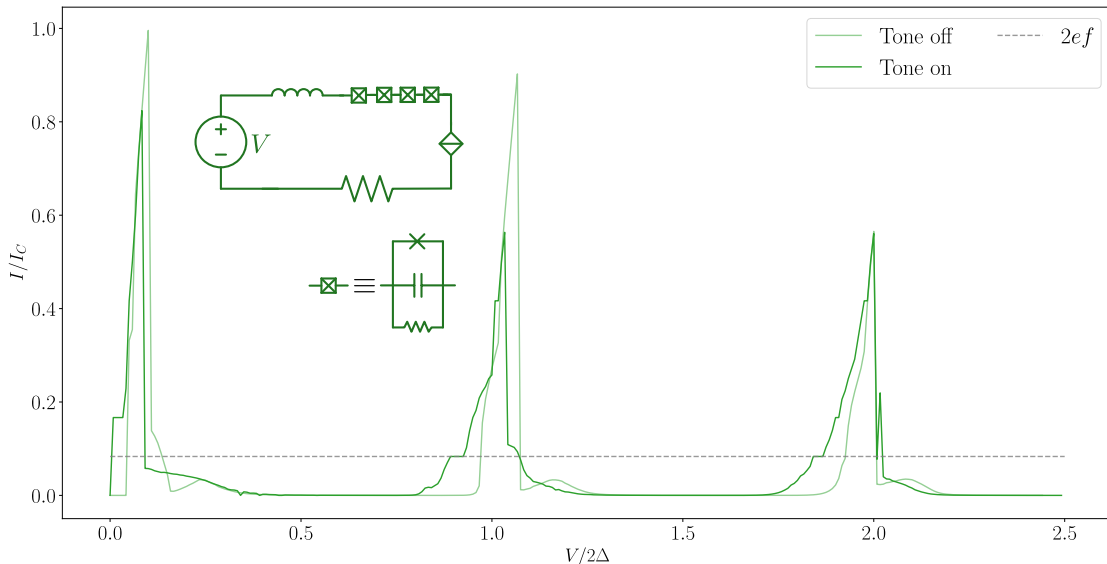


FIG. 7. Simulated IV curve of a chain of four junctions in series with an inductance, a resistor, and a non-linear capacitor with and without an AC drive of frequency f . Current plateaux of height $2ef$ are observed before each 2Δ current peak in qualitative agreement with the experimental observations.

voltage V by an equation similar to (3)

$$V = L\ddot{Q} + R\dot{Q} + V_C \sin\left(\frac{\pi}{e}Q\right) + \sum_i \dot{\phi}_i. \quad (5)$$

We then solve Eq. (4) and (5) using a Runge-Kutta method of order four with a time-step $dt = 0.02 RC$. We then average the current $\langle I_{\text{tot}} \rangle$ to obtain its DC component and plot the IV characteristic.

Due to the complexity of simulating the response of $N_a = 3500$ JJs, we focus on a system with $N = 4$ junctions embedded in a circuit with inductance $L = 5 \mu\text{H}$ which captures the inductance of the remaining JJs that form the superinductance.

Fig. 7 displays the IV characteristic for the chosen parameters, with and without an applied microwave tone. Many features that we observe in the experimental IV curve are qualitatively reproduced by the simulation. First, we observe current peaks, spaced by 2Δ , corresponding to the successive switching of junctions in the array. Second, when the microwave tone is applied we observe the formation of current plateaux just before the voltages at which the current peaks occur. These current plateaux are repeated for each current peak.

Other features of this simple simulation do not qualitatively match the experimental IV curves. Whereas the height of the simulated current peaks is of order I_c , and monotonically decreasing with voltage, the experimental current peaks are all well below the estimated I_c , with heights suppressed for small V_0 . This qualitative differ-

ence points to aspects of the UJJ, which is simplified in the model. The width of the simulated plateaux appear to be of order V_c , while experimentally we measure different widths, as is shown in Fig. 5.

Device and experimental setup

The device consists of Al/AIO_x/Al junctions in a microstripline geometry, fabricated with the shadow evaporation technique and electron beam lithography on a fused silica wafer. The substrate choice is related to the minimisation of ground capacitances which, being proportional to the dielectric constant, are reduced of about four-folds with respect to silicon. Reduced ground capacitance and large inductance produce a high impedance and prevent Landau-Zener transitions between Bloch bands which might suppress the amplitude of Bloch oscillations⁴⁰. Details on the fabrication procedure can be found in the data repository of this work⁵¹.

The superinductance is formed from JJs with capacitance $C_a \simeq 45 \text{ fF}$ and critical current $I_c \simeq 150 \text{ nA}$, estimated from their area by using the expected capacitance per unit of area $\sigma_C = 45 \text{ fF}/\mu\text{m}^2$ and critical current density of $\sigma_I = 15 \text{ A}/\text{cm}^2$, respectively. Each UJJ has an area of $0.04 \mu\text{m}^2$, from which we can similarly estimate a capacitance of $C = 1.8 \text{ fF}$ and a critical current of 6 nA .

A detailed schematic of the setup used in this work is reported in Fig. 8. The experimental apparatus can si-

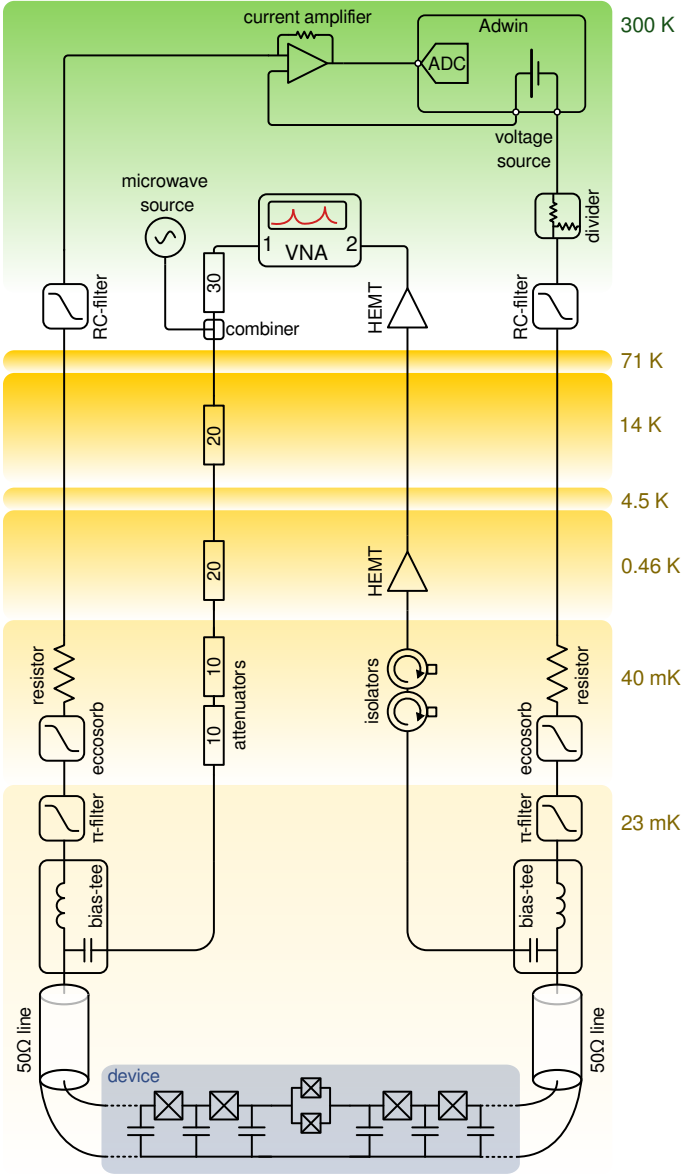


FIG. 8. Experimental setup used in this work. The yellow boxes show the different stages of the dilution refrigerator with their temperatures on the right side, while the part of the apparatus at room temperature is in green. The device is in gray at the bottom of the figure, the reader is referred to the main text for its description.

multaneously perform DC and RF measurements, as is shown in Fig. 2c. This is achieved using two off-chip bias-tees that decouple kHz frequency measurements from the ones in the GHz range. The two ports of the Bloch array are connected to the bias-tees via $50\ \Omega$ -matched lines. At the lowest temperature stage, the DC lines feature 45 MHz π -filters, $50\ \Omega$ damping resistors in series and Eccosorb filters. Further RC and π -filters are applied at room temperature, which are the main source of damping in the circuit. The current I_0 is amplified with a low noise transimpedance amplifier, while the readout and

voltage bias are performed with a real-time analog-to-digital converter (Adwin-Gold II).

The IV curves are collected by biasing the device with triangular voltage ramps with period ranging from 10 ms to 10 s, depending on the measurement conditions and voltage range. To apply a magnetic field on the sample we employ a superconducting coil anchored to the sample holder. The measured periodicity in the IV response agrees with what is estimated considering the SQUID area and the magnetic field produced by the coil. Microwaves are applied to the sample via a high frequency line with an attenuation of about 60 dB, which is connected to one of the bias-tees, while spectroscopic measurements are performed with extra 30 dB attenuation. The second bias-tee's high frequency port is connected to an isolator and then to a high electron mobility transistor (HEMT) amplifier working in the 4-8 GHz frequency range and with a noise temperature of about 5 K. Further amplification is performed at room temperature, before reading out the signal with a vector network analyser. The setup is housed in an inverted dilution refrigerator with a base temperature of 23 mK.

Full IV curve and flux dependence

The current-voltage characteristics of the Bloch array are reported in Fig. 9. Figure 9a shows the IV curves over the largest voltage span, with switching to the resistive branch of the whole array at a voltage of about $2N_a\Delta \simeq \pm 1.6\ \text{V}$, marked by a sharp peak in the device conductance. From this, we estimate $\Delta = 0.23\ \text{mV}$, compatible with the superconducting gap of aluminium thin films⁵². For applied voltages $V_0 \sim 4\ \text{V}$, we estimate the normal state resistance of each JJ in the array $R_a = 7.75\ \text{M}\Omega/N_a = 2.21\ \text{k}\Omega$. Since, the resistance of the UJJ is expected to be $\sim 20\ \text{k}\Omega$, its contribution to the total array resistance is negligible. Using Ambegaokar-Baratoff formula, $I_c = \pi\Delta/2R_a$, we estimate the critical current of the large junctions $I_c \simeq 164\ \text{nA}$, compatible with the estimation obtained with SEM imaging.

At applied voltages $V_0 < \pm 1.6\ \text{V}$ the IV has a more resistive branch and a central plateau of about $\Delta_s \simeq 1\ \text{V}$, where its resistance is larger than $100\ \text{M}\Omega$, as shown in Fig. 9b. This is in agreement with prior measurements and theory⁵³. At a lower voltage scale, see Figs. 3a and 9c, more features appear^{42,43}, whose explanation is reported in the main text. Current peaks are present when the voltage is an integer multiple of 2Δ , and their spacing is understood in terms of a sub-gap to resistive switching mechanism as explained in the main text.

Figure 9d displays the IV curve for the finest voltage scale. For $V_0 < \Delta$ we detect a low-voltage-current with non-trivial shape which we associate with a combination of supercurrent and inelastic Cooper pair tunnelling^{5,54,55}. Small applied magnetic fields are ex-

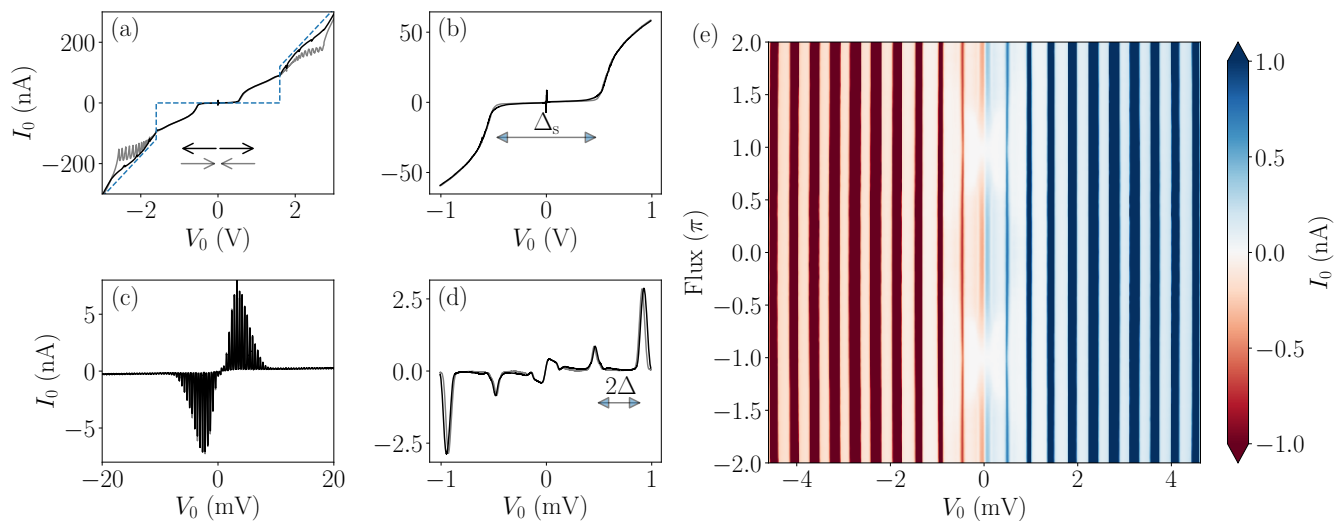


FIG. 9. Full IV curve of the Bloch array. Plots (a) to (d) show the IV curve at different scales. The black (grey) line indicates increasing (decreasing) $|V_0|$, as shown by the arrows in (a), while in the same plot the blue dashed line is a guide for the eye. The voltage scale is gradually reduced from (a) to (d); discrepancies between the current amplitude in the plots are related to measurement conditions. Finally, (e) shows the flux dependence of the Bloch array's IV characteristic at low voltages.

pected to tune the E_J/E_C ratio of the UJJ, while the superinductances, being formed of single junctions are to first order not affected. Figure 9e shows the flux dependence of the low voltage IV curve of the Bloch array, where at $\pm\pi$ flux we observe suppression of the low-voltage-current^{54,55}.

Microwave measurements of the Bloch array

Microwave spectroscopy is used to measure the resonances of the Bloch array¹⁶. In particular, we identify several peak doublets, which can be further studied with two-tone measurements⁵⁶. We probe the transmission of the array near one of the observed resonances at 4.13 GHz and sweep the power and frequency of an additional applied tone. When the tone is resonant with an additional mode of the array the transmission at the probe mode is affected. From these data we observe a free spectral range of about 1 GHz between two peaks doublets, and a JJ plasma frequency of 16 GHz, beyond which no modes are observed. From these measurements, we obtain the JJ inductance $L_a \simeq 1.9$ nH, capacitance $C_a \simeq 45$ fF, and ground capacitance $C_g \simeq 7 \times 10^{-4} C_a = 0.3$ aF. These results are in agreement with the ones obtained by measuring the dispersion relation of a JJ array resonator fabricated in the same batch.

We then obtain the two superinductance's impedance and inductance $\sqrt{L_a/C_g} = 8.0$ k Ω and $N_a L_a/2 = 3.3$ μ H. The critical current of the large JJs, $I_c = \hbar/2eL_a \simeq 173$ nA is in good agreement with the values estimated in the previous section. The spectroscopic data also give information on the UJJs. Referring to Fig. 3c, the observed

modes splitting yields a capacitance of about 1fF $\simeq C/2$, in agreement with the value estimated through the ultra-small junction's area.

The effect of V_0 on the S_{21} of this mode doublet is displayed in Fig. 10. Here, we see how a current flowing in the Bloch array degrades the microwave response of both modes, reducing the transmission. The microwave mode doublet is recovered when I_0 is close to zero, further confirming the interpretation of the IV curve reported in the main text.

Microwave modes used for observing current steps

To observe the steps at different frequencies of the microwave tone, we identified the suitable peak doublets and their response to the microwave tone using the method displayed in Fig. 4b. The corresponding power dependence for the other observed steps are displayed in Figure 11. In each case, the characteristic shape of the power response guides the choice of p to observe the steps. A summary of the identified frequencies and powers suitable for the emergence of the steps is reported in Table II. Referring to Fig. 5c, we note that the 5 GHz step is not displayed since the corresponding IV curve suffers from a much higher noise with respect to the other three. Repeated measurements show that with this tone frequency, the Bloch array experiences a significant $1/f$ noise which, shifting the position of the peaks during the measurement, compromises the averaging reliability. For this reason the averaging performed on this curve is extremely limited, leading to a higher current noise, as can be seen from the errorbar in the inset of Fig. 5c.

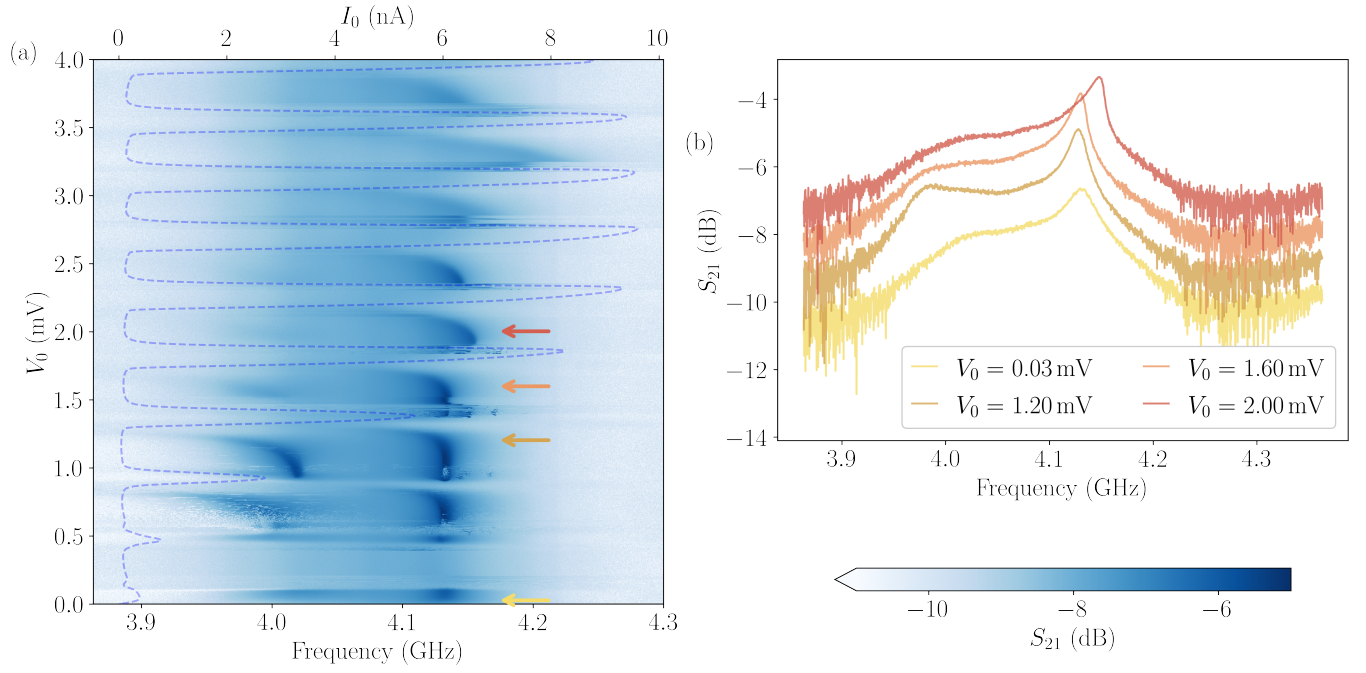


FIG. 10. Plot (a) is the variation of the transmission with respect to V_0 , where the IV was superimposed to the plot as a dashed line for illustrative purposes. In (b) we show slices of (a) at different voltages, where a 1 dB offset for each curve is added for clarity.

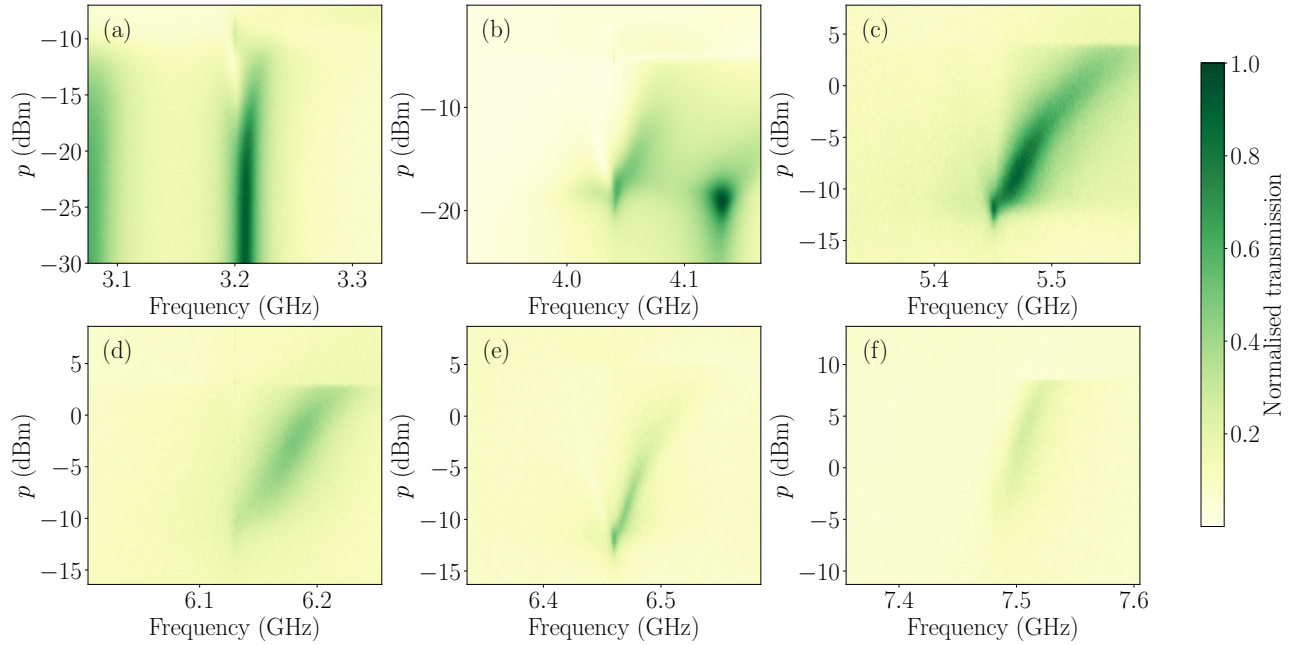


FIG. 11. Power sweep on the peak doublet for some of the modes identified in the Bloch array, ranging from (a) at 3.2 GHz to (f) at 7.5 GHz. These measurements are used to identify the power to use to obtain the steps.

f	p
3.20 GHz	-11.1 dBm
4.04 GHz	-5.0 dBm
5.45 GHz	2.8 dBm
6.11 GHz	Not identified
6.46 GHz	3.8 dBm
7.48 GHz	Not identified

TABLE II. Microwave tone parameters used to observe the steps in Fig. 5, obtained through the measurements in Fig. 11.